Lattice study of the incommensurate ω phase transition in Zr-Nb alloys

H. Kubo[1] and S. Farjami[2]

[1]*Kanto Polytechnic University, 612-1 Mitake Yokokura, Oyama 323-0810, Japan*

[2]*National Institute for Materials Science, Sengen 1-2-1, Tsukuba, Ibaraki 305-0047, Japan*

(Received 1 February 2010; revised manuscript received 18 November 2010; published 7 April 2011)

The stability of the incommensurate ω phase has been studied in the scheme of the Landau-Lifshitz (L-L) free-energy model reformed for the weak first-order phase transition. It is revealed that the negative third-order term of the L-L expansion drives the transition and works, in competition with the second-harmonic term, to form the modulated ω phase; moreover, it functions to maintain soliton walls with constant width against temperature changes. The modulated ω phase is elucidated to have a microstructure with the sequence of subvariants—ω1-ω3-ω2—separated by soliton walls of anti-ω structure. A series of primitive activation units of the modulated ω phase, which can be depicted in a phase diagram, is obtained in the Zr-20 wt% Nb-alloy system by analyzing the L-L free-energy function with the appropriate numerical calculations.

DOI: 10.1103/PhysRevB.83.134302 PACS number(s): 64.70.K−, 05.70.Fh

I. INTRODUCTION

It is well known that the bcc phase (β) of Group IVb (Zr, Ti, Hf) transition metals exhibits inherent lattice instabilities, which manifest themselves with the existence of a distinct dip in the LA phonon branch at the reduced wave vector $\mathbf{k}_\omega = 2\pi\xi(111)$ for $\xi = 2/3$.[1–4] Because of the intrinsic instability of the lattice, bcc transition metals of Group IVb and their alloys yield metastable states of the ω phase with modulated structures and tend to undergo structural phase transitions in the temperature range $T_i > T > T_C$ below the metastable ω phase starting temperature T_i and above the stable ω phase starting temperature T_C. This structural phase transition occurs in the scheme of the weak first-order structural transitions but is similar to the second-order phase transition.[2–6]

In a phase diagram, the lines of T_i and T_C must meet at a point L on the line T_ω separating the disordered state (β) from the simple ordered state (ω) in a construction reminiscent of the axial nearest-neighbor Ising (ANNI) model[7,8] or Frenkel-Kontrowa model[7] in which a Lifshitz point L is found at the junction of three lines. In the metastable ω phase transition, the nearest-neighbor interaction between the close-packed planes is $J_1 > 0$, but the interaction between planes of the next-nearest neighbors is $J_2 < 0$. Therefore, as was theoretically found to be true for the ANNI model, should the modulated ω region in the phase diagram also contain an infinite number of modulated structures? Then, the subject we are concerned with is to describe the possible modulated ω phase and to clarify the kinematic stabilizing mechanism that occurs in the metastable ω phase transition on the basis of the pertinent thermodynamical model of the weak first-order phase transition.

The original fundamental analysis for the stable ω phase transition has been performed by Ho *et al.*[1] in the first-principles calculations of the crystal lattice energy. They have demonstrated quite clearly that the transition from the β to the stable ω phase can occur by weak first-order structural transitions. However, their calculations are true only for the stable ω phase. The analysis of the metastable ω phase transition has been preceded by Cook,[5] de Fontaine,[2] Pynn,[9] and Horovitz *et al.*[10]

Cook[5] set up a Landau-type thermodynamical potential (free energy) on the basis of continuum model theory for the incommensurate ω phase transition. He asserted the importance of the distinct dip in the [111]LA phonon branch with the minimum phonon energy exhibited at the reduced wave vector $\mathbf{k}_m$, which is slightly deviated from the ideal ω point $\mathbf{k}_\omega$ to higher angles. He also emphasized that the $\mathbf{k}_\omega$ wave itself possesses a unique property, shared by no other: Acting alone, $\mathbf{k}_\omega$ is the only wave vector that can produce a nonvanishing third-order term in the Landau-Lifshitz (L-L) expansion of free energy. A competition occurs between the initial harmonic wave with the wave vector $\mathbf{k}_m$ and the anharmonic one with the wave vector $\mathbf{k}_\omega$. It results in a long-period structure (incommensurate structure) of alternating layers of ω and β phases. This is Cook's model[5] of the modulated ω phase and the kinematic stabilizing mechanism for the metastable ω phase of the incommensurate phase (IC) structure (IC ω phase).

On the other hand, on the basis for the discrete lattice model of a two-state system $\sigma_i = 0, 1$, Horovitz *et al.*[10] predicted the metastable ω phase as a class of phase with incommensurate structure, which consists of commensurate ω regions $\sigma_i = 1$ but is separated by soliton walls of β phase $\sigma_i = 0$. The phase (ϕ)-dependent Hamiltonian is set up with a strong locking energy $V_{\text{lock}} = \omega_0^2[1 - \cos(3\phi)]$, which is supposed to be derived from the lattice discrepancy between the parent and the product phase. This stacked soliton structure reproduces a very particular sequence of subvariants, –ω1-ω3-ω2–, in accordance with the result obtained from x-ray diffraction experiments by Borie *et al.*[11]

Thus, one result is the long-period structure of the ω and β layers proposed by Cook,[5] determined by setting up a L-L free energy with the third-order term, and the other is the stacked soliton structure proposed by Horovitz *et al.*,[10] determined by setting up the Hamiltonian with a strong locking energy term. There is also a discrepancy between the kinematic stabilizing mechanisms. In the former result, the transition is driven by the third-order term of the free energy in the L-L expansion, and in the latter, it is driven by the second-order term. Furthermore, the ANNI model is a two-state model (spin up, spin down; $\sigma_i = \pm 1$), but the ω case is a three-state model

(displacement forward, backward, none; $\sigma_i = 0, \pm 1$). This still seems confusing, even when beginning from the analysis of phase stability in the metastable ω phase.

It is clear from the above arguments that, to obtain a pertinent thermodynamical model for the metastable ω phase transition, we are obliged to set up the Hamiltonian or thermodynamical potential with adequate order parameters (σ_i, η, ϕ, ε_{ij}, etc.), including, of course, the proper component in the transition. Herein, therefore, a group-theory consideration is made first to survey the necessary order parameters for the weak first-order phase transition of the IC ω phase and to consider the crystallographic symmetry for the L-L phenomenological theory (Appendix A). The thermodynamical potential energy is represented as the sum of the two different kinds of potential terms: the phonon-originating components (phonon amplitude η, the phase change of phonon ϕ_n, and their derivatives) and the static strain-originating components (Bain distortion ε_{ii}, Burgers distortion ε_{ij}, and their derivatives). These components are successively optimized in the Zr-20 wt% Nb (Zr-20 Nb) alloy. The optimization of the phonon-originating components is discussed in Sec. II to identify the microstructure of the metastable ω phase. In Sec. III, the static strain-originating components are estimated using microscopic elasticity theory to identify the size and shape of the metastable ω phase. In Sec. IV, a prediction of the temperature dependence of the metastable ω structure is made from the minimized thermodynamical potential. In Sec. V, the diffuse scattering spectra are examined to confirm the soliton model for the metastable ω structure. Sec. VI is devoted to discussions.

II. OPTIMIZATION OF PHONON-ORIGINATING COMPONENTS

There are four equivalent $\langle 111 \rangle$ directions in the β phase, but for simplicity, we focus on the lattice arrangements in the particular [111] variant ($\lambda = 1$ in Appendix A) of the IC ω phase. Therefore, the crystal is supposed to consist of discrete (222) lattice planes in the quasi-one-dimensional model. Coarse graining is performed in each (222) plane with two-dimensional scaling.

The IC ω phase transition is described by the incomplete phonon softening in the irreducible E_g representation of the space group $Im\bar{3}m$. Therefore, in the analysis of the thermodynamical potential energy, we must take the order parameters of the phonon-originating components (intracellular distortion) and the static strain-originating components (intercellular distortion) into account. The former order parameter, $Q = \eta \exp[-i\phi]$ for $\lambda = 1$, which describes the phase-dependent amplitude of the transformation wave, constitutes the functions (A8), (A9), and (A14), and the latter order parameter, i.e., the Bain distortion (ε_{xx},ε_{yy},ε_{zz}) and the Burgers distortion (ε_{xy},ε_{yz},ε_{zx}), comprises Eqs. (A12) and (A14) and Eqs. (A10) and (A14), respectively. Because the basis function of the Bain distortion is not mixed with the basis function (ε_{xy},ε_{yz},ε_{zx}) of T_{2g}, we can initialize the IC ω phase transition by fifth-order parameters η, ϕ, and ε_{ii} ($i = x,y,z$), and their derivatives. Including terms up to the sixth order in the proper component η, we find the thermodynamical potential-energy (free-energy) density $g(\eta,\phi,\varepsilon_{ii})$ of Eq. (A7),

$$\mathrm{g}(\eta,\phi,\varepsilon_{ij}) = g_Q(\eta,\phi) + g_Q^g(\eta) + g_{\mathrm{strain}}^{\mathrm{Bn}}(\varepsilon_{ij}) + g_{\mathrm{strain}}^{g}(\varepsilon_{ii}) + g_{Q-\mathrm{strain}}(\eta,\varepsilon_{ii})\ (\mathrm{eV/atom})\,. \tag{1}$$

From Eq. (A8), we obtain the following expression for the thermodynamical potential-energy density $g_Q(\eta,\phi)$ for a weak first-order phase transition in the quasi-one-dimensional model,

$$g_\psi(\eta,\phi) = \tfrac{1}{2}A_0\eta^2 + \tfrac{2}{3}B_0\eta^3\cos(3\phi) + \tfrac{1}{4}C_0\eta^4 + \tfrac{2}{5}E_0\eta^5\cos(3\phi) + \tfrac{1}{6}\eta^6[D_0 + 2D_1\cos(6\phi)]. \tag{2}$$

The symmetry operation $\{E|\mathbf{n}\}$ of Eq. (A3) identifies the number $p = 3$ and 6 of the cos $(p\phi)$ term of Eq. (2). However, hereafter, the fifth-order term will be omitted because of the weak first-order phase transition ($|E_0\eta^5| \ll |B_0\eta^3|$). Adopting the expression of the local strain field $\eta(\mathbf{n})$ and $\phi(\mathbf{n})$, we can express the gradient term from Eq. (A9) as follows:

$$g_Q^g(\eta) = \left[-\kappa\hat{\boldsymbol{n}}\cdot\nabla\phi + \frac{\chi}{2}(\hat{\boldsymbol{n}}\cdot\nabla\phi)^2\right]\eta^2 + \frac{\chi}{2}(\hat{\boldsymbol{n}}\cdot\nabla\eta)^2\,, \tag{3}$$

where $\hat{\boldsymbol{n}}$ is the unit vector in the [111] direction. The notation $\nabla\phi$ is used throughout the present paper only for convenience, but in this section of the discrete lattice model, $\nabla\phi$ should be replaced by the discrete lattice notation as $\nabla\phi \equiv [\phi(\mathbf{n}+1) - \phi(\mathbf{n})]/\mathbf{d}$, $\mathbf{d}$ representing the crystal lattice vector between the lattice point n and $n+1$.

We minimize the thermodynamical potential-energy density with respect to ε_{ii} ($i = x,y,z$) in a similar manner as that demonstrated for dielectric materials.[12] As a result, the thermodynamical potential-energy density, Eq. (1), is expressed in a form that eliminates $g_{Q-\mathrm{strain}}(\eta,\varepsilon_{ii})$, for example, by modifying the coefficients C_0 in the function (2) as $C = C_0 - A_{\mathrm{Bn}-\psi}^2/c_{11}$. The function (2) is minimized when the phase change of stacking ϕ takes the following values:

$$\phi = 0,\ \pm\frac{2m\pi}{3} \qquad (m = \text{integer}). \tag{4}$$

The above condition for the minimum thermodynamical potential-energy density leads to the conclusion that discommensuration takes place along the [111] direction with the formation of soliton walls.

A. Soliton solution

By summing the potential-energy density $g(\eta,\phi,\varepsilon_{ii})$ over the crystal, we obtain the thermodynamical potential energy of the system,

$$G(\phi) = \frac{1}{\Omega}\int_V g\left(\eta,\phi,\varepsilon_{ij}\right)dV \quad (\mathrm{eV}/N\ \text{atoms})\,, \tag{5}$$

where Ω is the atomic volume. The minimum thermodynamical potential energy with respect to the phase field ϕ can be obtained using the Euler equation, which describes

the equilibrium energy state of the system. We obtain the differential equation for the phase field $\phi(n)$ as

$$\chi \eta_\omega^2 \hat{\boldsymbol{n}} \cdot \nabla (\hat{\boldsymbol{n}} \cdot \nabla \phi) = -2B_0 \eta_\omega^3 \sin(3\phi) - 2D_1 \eta_\omega^6 \sin(6\phi), \tag{6}$$

where the terms on the right-hand side (RHS) represent the locking potential energy. h_w is the stress-free strain for the IC ω phase formation. Equation (6) is a double sine-Gordon equation for $\phi(\mathbf{n})$. The solution of this double sine-Gordon equation is, understandably, not apparent[13] compared to the simple sine-Gordon equation.[10–14]

Integrating Eq. (6) once and utilizing the characteristic form of the double sine-Gordon equation, we obtain the integral form of the phase field $\phi(\mathbf{n})$, as follows:

$$n(222) = \frac{2}{d_{111}\sqrt{z}} \int_0^\phi \frac{1}{\left[1 - b \sin^2\left(\frac{3}{2}\phi\right) + a \sin^4\left(\frac{3}{2}\phi\right)\right]^{1/2}} d\phi, \tag{7}$$

where $n(222)$ indicates the number of atomic layers along the [111] direction and d_{111} is the interplanar distance of (111) planes. a and b are defined as $a \equiv 16D_1\eta_\omega^4/3zx$ and $b \equiv 8(B_0\eta_\omega + D_1\eta_\omega^4)/3zx$, respectively. z is the integration constant that represents the square of the first derivative of $\phi(\mathbf{n})$ at $\mathbf{n} = 0$, i.e., $z = (\hat{\boldsymbol{n}} \cdot \nabla\phi)^2_{n=0}$. Equation (7) takes on the form of a complete elliptic integral of the first kind if the higher-order term a is ignored. However, it should be noted that $b < 0$ in Eq. (7). This causes significant differences in the behavior of the present IC from that derived from $b > 0$. It is also important to recognize that the factor B_0 in the coefficient b does not depend on temperature because the entropy term is only involved in the even-order terms of the L-L free energy [see Eq. (B8)].

Numerical integration of Eq. (7) is carried out to understand the intuitive behavior of $\phi(\mathbf{n})$. At sufficiently high temperature T close to T_i, the plane-wave approximation (PWA) of the phase field holds as $\phi(n) = \Delta\mathbf{k}_\omega \cdot \mathbf{n} + \phi^0$ via $\hat{\boldsymbol{n}} \cdot \nabla(\hat{\boldsymbol{n}} \cdot \nabla\phi) = 0$ of Eq. (7). This reveals that, although the harmonic term A_0 does not appear in Eq. (7), it affects the formation of the modulated ω phase through $\Delta\mathbf{k}_\omega$. As mentioned by Cook,[5] a competition occurs between the initial harmonic wave with the wave vector $\mathbf{k}_m$ and the anharmonic one with the wave vector $\mathbf{k}_\omega$. The calculation is initiated by estimating the numerical values of a and b at $T = 1200$ K. The PWA provides the relation $D_1 = -B_0/2\eta_\omega^3$, then, $b = 0$. The disposable parameter D_1 is estimated from the numerical calculation by adjusting it for Eq. (7) to take $n(222) = 33$ at 1200 K.[15–17] The obtained value $D_1 = 0.552$ (eV/atom) gives the third-order energy coefficient of the L-L free energy as $B_0 = -0.210$ (eV/atom). The trajectory of the phase field $\phi(\mathbf{n})$ for $T = 1200$ K close to T_i is produced with the numerical values $a = 37.0\,\text{nm}^{-2}$ and $b = 0\,\text{nm}^{-2}$, which are obtained from D_1 with an equilibrium degree of order $h_w = 0.575$,[16,17] the gradient coefficient $\chi = 0.0087\ \text{nm}^{-2}\ \text{eV}^{-1}$/atom evaluated from the elastic energy modulus (EEM) [see Eq. (25) in Sec. III] and $z = 0.860$, which is obtained also at 1200 K from the relation $z = |\mathbf{k}_\text{m} - \mathbf{k}_\omega|^2 = (0.030\,|\mathbf{g}_{111}|)^2$ ($|\mathbf{g}_{111}|$ being the length of the [111] reciprocal lattice vector). Figure 1 shows the trajectory of $\phi(\mathbf{n})$ for $n(222) = 33$ at $T = 1200$ K close to T_i,

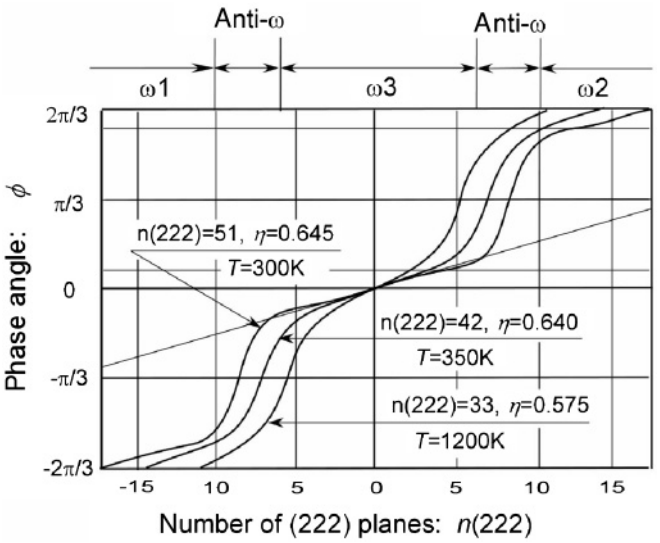

FIG. 1. The nonlinear phase change $\phi(\mathbf{n})$ is obtained by solving the double sine-Gordon equation in the quasi-one-dimensional IC ω phase in the Zr-20 Nb alloy.

$n(222) = 42$ at $T = 350$ K, and $n(222) = 51$ at $T = 300$ K. An alternating domain variant –ω1-ω3-ω2– is formed in sequence in the discommensurated ω phase. The phase appears to consist of thick solitons.

The phase field $\phi(\mathbf{n})$ for $T = 300$ K, which is close to $T_c = 280$ K,[5,18] is obtained from the numerical values $a = 49.9\,\text{nm}^{-2}$ and $b = 7.88\,\text{nm}^{-2}$, which are obtained without assuming the PWA and by keeping the third-order energy coefficient $B_0 = -0.209$ eV/atom constant, i.e., that common to all temperatures. The degree of order $h_w = 0.653$[5,16–18] and the square of the slope $z = 0.413$ are taken from experimental results.[16–18] Moving lower into the incommensurate phase, the ground-state configurations are described by a multisoliton lattice that separates nearly commensurate regions. Over the temperature range from 1200 to 300 K, the soliton width is kept nearly constant, whereas, the average inclination of $\phi(\mathbf{n})$ becomes continuously smaller with decreasing temperature, descending toward the straight line $\phi(\mathbf{n}) = \Delta\mathbf{k}_\omega \cdot \mathbf{n} + \phi^0$ at 300 K. These characteristics of the constant soliton width and the average inclination of $\phi(\mathbf{n})$ are particularly different from the behavior of incommensurate structures of even-order transition (the transition with no odd-order terms included in L-L expansion), e.g., with $p = 10$ for $[N(CH_3)_4]_2ZnCl_4$, $p = 6$ for Rb_2ZnCl_4 and $p = 4$ for $(NH_4)_2BeF_4$.[14,19]

The soliton width n_wall (222) has often been estimated from the maximum slope of the trajectory $\phi(\mathbf{n})$ via the equation $(\mathbf{n} \cdot \nabla\phi)_\text{max}[(d_{111}/2)n_\text{wall}(222)] = 2\pi/3$, as

$$n_\text{wall}(222) = \frac{2}{d_{111}} \frac{2\pi}{3} \left(\frac{3\chi}{3\chi - 8\,B_0\,\eta_\omega}\right)^{1/2}. \tag{8}$$

The term $-8B_0\eta_\omega > 0$ of Eq. (8) is dedicated to maintaining the soliton width constant over the temperature range $T_I > T > T_C$, viz., the decrease of z value with the temperature is compatible with the increase in $\eta_\omega \propto (T_1 - T)^\beta$. This is in contrast to the studies[14,18] that report that, for even-order transitions, the soliton width decreases precipitously with decreasing temperature. The soliton width, here, is estimated

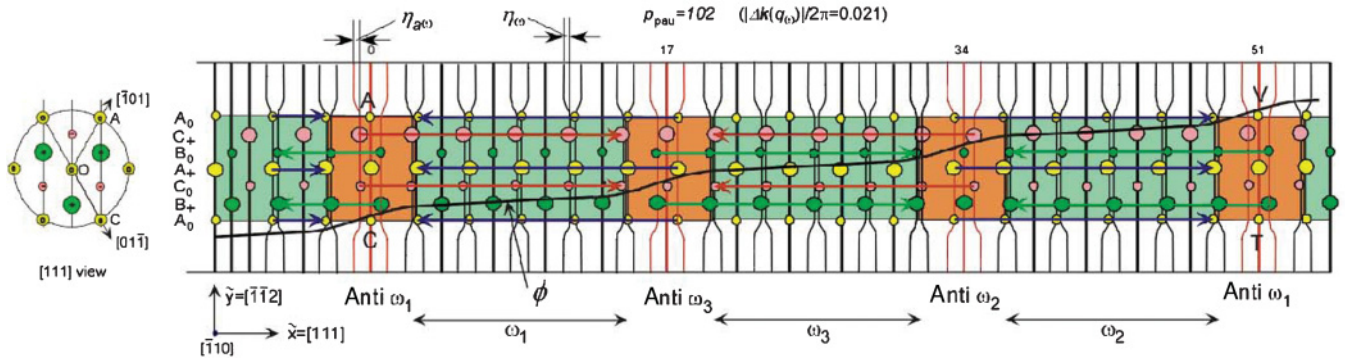

FIG. 2. (Color online) Schematic of the microstructure of the IC ω phase obtained by solving the sine-Gordon equation for the phase field ϕ. The sequence of subvariants $-\omega_1$-ω_3-ω_2- is separated by the anti-ω phase (soliton walls).

from Eq. (8) as $n_{\rm wall}(222) \sim 3.3$ at 1200 K and 3.1 at 300 K. This information and a gradual phase change of $\phi(\mathbf{n})$ at the commensurate parts provoke an image of a microstructure composed of solitons consisting of an anti-ω phase structure (anti-ω wall model) as the core part of the incommensurate region rather than a flat β phase structure (β wall model by Horovitz *et al.*). In fact, as will be elucidated in Sec. V, the diffuse intensity spectra obtained from experiments could be explained by the anti-ω model. The product phase speculated by this nonlinear phase change is depicted schematically in Fig. 2 for $n(222) = 51$ at 300 K with a single anti-ω wall, i.e., $n_{\rm wall}(222) = 3$. However, the microstructure is unwound by lattice distortions, according to the phase change depicted by $\phi(\mathbf{n})$ in Fig. 1. Therefore, for the thick solitons of $n(222) = 51$, we could eventually take the dimension of the soliton walls as $n_{\rm wall}^{\rm thick}(222) = 7$, the region extended on both sides of the core anti-ω wall bounded by the two planes, which are identified by the zero-curvature points on the trajectory of $\phi(\mathbf{n})$.

In the structural model of Fig. 2, the chain of atoms in the $(\bar{1}\bar{1}2)$ atomic planes is supposed to be displaced uniformly by $\pm(d_{111}/2)\eta_\omega$ along the [111] direction. This unique displacement of each chain of atoms is demonstrated by the arrows in Fig. 2. We define the primitive activation unit $p_{\rm pau}$ as the number of atoms to be activated in a single jump process in the heterophase fluctuation of the IC ω phase. Then, the number of atoms $p_{\rm pau} = 102$ is counted in the unit cell of $n(222) = 51$ existing in the square region ACTV in Fig. 2. The anti-ω wall is regularly introduced into the IC ω phase. Each ω subvariant measures approximately $n(222) \approx 14$ planes ($\sim$1.4 nm) in thickness in the model. This is in good agreement with the experimental findings of Dawson and Sass, who reported on coaxial ω particles with lengths of 1.0–1.5 nm, with three to six particles per row.[18] This general feature of commensurate regions separated by discommensurations (or soliton walls, producing phase shift) is common to many long-period structure models.[14,19,20]

III. OPTIMIZATION OF STRAIN-ORIGINATING COMPONENTS

The IC ω embryo is formed coherently in the parent phase and yields the elastic strain energy in three-dimensional fields. Therefore, the thermodynamical potential-energy density $g(\eta,\phi,\varepsilon_{ii})$ should be treated by three-dimensional fields.

The location-dependent pseudospin $\sigma(\mathbf{n})$ for the atom is defined as $\sigma(\mathbf{n}) = 1$ if the defect atom is located at site $\mathbf{n}$ with stress-free strain $+\eta_\omega > 0$ and $\sigma(\mathbf{n}) = -1$ for the defect atom with stress-free strain $-\eta_\omega < 0$; this pseudospin $\sigma(\mathbf{n})$ vanishes for the defect atom with no displacement (cf. Fig. 2).[21–24] Using the pseudospin $\sigma(\mathbf{n})$, we can define the local strain field $\eta(\mathbf{n}) = \eta\sigma(\mathbf{n})$. The Fourier-transformed (FT) pseudospin $\sigma(\mathbf{k})$ is defined as

$$\sigma(k) = \frac{1}{p_{\rm pau}} \sum_{n=1}^{p_{\rm pau}} \sigma(\mathbf{n}) \exp(-i\mathbf{k}\cdot\mathbf{n}), \tag{9}$$

where the FT is purposely executed within a primitive activation unit of the IC ω phase, instead of the whole crystal.

The shape of the IC ω embryo can be expressed by the defect probability $\theta(\mathbf{n})$, which is defined as $\theta(\mathbf{n}) = 1$ if the defect atom is located at site $\mathbf{n}$ within the IC ω embryo and vanishes at site $\mathbf{n}$ outside the IC ω embryo. Using the defect probability $\theta(\mathbf{n})$, we can define the local strain field $\varepsilon_{ii}(\mathbf{n}) = \varepsilon_{ii}\theta(\mathbf{n})$. Using the FT pseudospin $\sigma(\mathbf{k})$ and the FT defect probability $\theta(\mathbf{k})$, we can define the FT strain moment of the Bain distortion $\varepsilon_{ii}(k)$ and that of the ω distortion $\eta(\mathbf{k})$ as follows:

$$\varepsilon_{ii}(\mathbf{k}) = \varepsilon_{ii}\theta(\mathbf{k}), \quad \text{and} \quad \eta(\mathbf{k}) = \eta\sigma(\mathbf{k}). \tag{10}$$

The FT defect probability for shape is often called the shape function $\theta(\mathbf{k})$ in the microscopic theory of elasticity. It represents the FT IC ω embryo and gives the space correlation function $C(\mathbf{k})$ in the form $C(\mathbf{k}) = [(N_{\rm unit}/N)^2\theta(\mathbf{k}) - 1]^2$ in reciprocal space (k space), N being the total number of atoms in the crystal.

A. Equilibrium displacement

Knowing the lattice Green function $\Phi_{ij}^{-1}(-\mathbf{k})$ in k space, we can express the FT displacement $U_i(\mathbf{k})$ at the mechanical equilibrium as follows:[25]

$$2U_i(\mathbf{k}) = \Phi_{ij}^{-1}(-\mathbf{k})\Psi_j^{\rm Bn}(-\mathbf{k})\tau(\mathbf{k}) + \Phi_{ij}^{-1}(-\mathbf{k})\Psi_j^{\omega}(-\mathbf{k}) \times [\tau(\mathbf{k}-\mathbf{k}_m) - \tau(\mathbf{k}+\mathbf{k}_m)], \tag{11}$$

where the function $\Psi_j^{\rm Bn}(-\mathbf{k})$ is the Bain-distortion component of the force yielded by the defect source (IC ω embryo) in the crystal and $\Psi_j^{\omega}(-\mathbf{k})$ is the ω-distortion component of the force.

The implicit summation is assumed for the repeated suffixes of the Cartesian coordinates i and j. In the present defect system, $(\mathbf{k})$ is the FT product term of $\theta(\mathbf{n})\delta(\mathbf{n})$, which is expressed in a convoluted form in the Fourier space as follows:

$$\tau(\mathbf{k}) = \sum_{h} \theta(\mathbf{h})\,\sigma(\mathbf{h}-\mathbf{k}). \tag{12}$$

This $\tau(\mathbf{k})$ is the defect amplitude in the IC ω phase system.[22,25] It should be noted that the defect amplitude $\tau(\mathbf{k})$ of the first term on the RHS of Eq. (11) yields a sharp symmetric peak for the product $\tau(\mathbf{k})\tau^*(\mathbf{k})$ at the Γ point in k space and the second term for the product $\tau(\mathbf{k}\pm\mathbf{k}_m)\tau^*(\mathbf{k}\pm\mathbf{k}_m)$ at $\pm\mathbf{k}_m$ point in k space.

The inverse of the lattice Green function $\Phi_{ij}(\mathbf{k})$, which is often called lattice coupling parameter (CP) in microscopic elasticity theory, is related to the dynamical matrix of the parent phase by $\Phi_{ij}(\mathbf{k}) = mD_{ij}(\mathbf{k})$, where m represents the effective mass of an atom of the alloy.

The analytical expression of $\Psi_j^{\mathrm{Bn}}(-\mathbf{k})$ is obtained in a form proportional to the derivative of the lattice CP,[23,26]

$$\Psi_j^{\mathrm{Bn}}(-\mathbf{k}) = i\hat{\varepsilon}_{ii}a_i\frac{\partial\Phi_{ij}(\mathbf{k})}{\partial k_i}. \tag{13}$$

The FT force $\Psi_j^{\omega}(-\mathbf{k})$ for the ω distortion is given in a form directly proportional to the lattice CP as[5,25]

$$\Psi_j^{\omega}(-\mathbf{k}) = i\left(\frac{\eta_\omega}{12\sqrt{3}}\right)a_i\Phi_{ij}(\mathbf{k}). \tag{14}$$

B. Elastic strain energy

The elastic strain energy density yielded by the distortion wave (transformation wave) with the wave vector $\mathbf{k}$ is obtained using the FT displacement $U_i(-\mathbf{k})$ as follows:

$$g_{\mathrm{elastic}}(\mathbf{k}) = \tfrac{1}{2}\Phi_{ij}(\mathbf{k})\,U_i(\mathbf{k})\,U_i(-\mathbf{k}), \tag{15}$$

where $g_{\mathrm{elastic}}(\mathbf{k})_{k\to 0} = g_{\mathrm{strain}}(\varepsilon_{ij})$. This strain energy density is composed of three different kinds of potentials: Bain-distortion energy $g_{\mathrm{elastic}}^{\mathrm{Bn}}(\mathbf{k})$, ω-distortion energy $g_{\mathrm{elastic}}^{\omega}(\mathbf{k})$ and interaction energy $g_{\mathrm{elastic}}^{\omega-\mathrm{Bn}}(\mathbf{k})$.

$$g_{\mathrm{elastic}}(\mathbf{k}) = g_{\mathrm{elastic}}^{\omega}(\mathbf{k}) + g_{\mathrm{elastic}}^{\mathrm{Bn}}(\mathbf{k}) + g_{\mathrm{elastic}}^{\omega-\mathrm{Bn}}(\mathbf{k}) \tag{16}$$

Summing up over $\mathbf{k}$, i.e., $\Sigma_k g_{\mathrm{elastic}}(\mathbf{k})$, for these three elastic strain energies, we can obtain the elastic strain energy of the crystal.

The first term on the RHS of Eq. (16) is the ω elastic strain energy density $g_{\mathrm{elastic}}^{\omega}[\eta_\omega(\mathbf{k}]$, which represents the elastic strain energy density associated with the stress-free ω distortion η_ω of the IC ω embryo. We obtain the analytical expression of $g_{\mathrm{elastic}}^{\omega}(\mathbf{k})$ from Eqs. (11), (14), and (15) as follows:

$$g_{\mathrm{elastic}}^{\omega}(\mathbf{k}) = \tfrac{1}{2}[\tau^2(\mathbf{k}-\mathbf{k}_m) + \tau^2(\mathbf{k}+\mathbf{k}_m)], \tag{17}$$

$$Y(\mathbf{k}) = -2\left(\frac{1}{2i}\frac{1}{6\sqrt{3}}\right)^2 a_i a_j \Phi_{ij}(\mathbf{k}). \quad (\mathrm{eV/atom}). \tag{18}$$

To evaluate the ω EEM $Y(\mathbf{k})$, the model pseudopotential method is adopted. The effective pair interactions are represented by an oscillatory potential arising from the mild

TABLE I. Interatomic force constants, $\varphi_{ij}(x)$, of the Zr-20 wt% Nb alloy obtained from the model pseudopotential method. Those obtained for pure Zr by Heiming *et al.*[27] are cited for comparison. Values are in units of N/m.

x_1(h,k,l) $\varphi_{ij}(x_i)$	$x_1(1/2,1/2,1/2)$ $\varphi_{ij}(\mathbf{x_1})$	$x_2(1,0,0)$ $\varphi_{ij}(\mathbf{x_2})$	$x_3(1,1,0)$ $\varphi_{ij}(\mathbf{x_3})$	$x_4(3/2,1/2,1/2)$ $\varphi_{ij}(\mathbf{x_4})$	$x_5(1,1,1)$ $\varphi_{ij}(\mathbf{x_5})$
Zr-20Nb Present paper	$\begin{pmatrix} 5.542 & 8.125 & 8.125 \\ 8.125 & 5.542 & 8.125 \\ 8.125 & 8.125 & 5.542 \end{pmatrix}$	$\begin{pmatrix} 12.179 & 0 & 0 \\ 0 & 0.159 & 0 \\ 0 & 0 & 0.159 \end{pmatrix}$	$\begin{pmatrix} 0.394 & 0.670 & 0 \\ 0.670 & 0.394 & 0 \\ 0 & 0 & -0.275 \end{pmatrix}$	$\begin{pmatrix} 0.543 & 0.137 & 0.137 \\ 0.137 & 0.178 & 0.045 \\ 0.137 & 0.045 & 0.178 \end{pmatrix}$	$\begin{pmatrix} -0.347 & -0.458 & -0.458 \\ -0.458 & -0.347 & -0.458 \\ -0.458 & -0.458 & -0.347 \end{pmatrix}$
Zr Heiming *et al.*[27]	$\begin{pmatrix} 7.351 & 8.565 & 8.565 \\ 8.565 & 7.351 & 8.565 \\ 8.565 & 8.565 & 7.351 \end{pmatrix}$	$\begin{pmatrix} 4.967 & 0 & 0 \\ 0 & -1.952 & 0 \\ 0 & 0 & -1.952 \end{pmatrix}$	$\begin{pmatrix} 0.615 & 1.524 & 0 \\ 1.524 & 0.615 & 0 \\ 0 & 0 & -2.083 \end{pmatrix}$	$\begin{pmatrix} 0.425 & -0.091 & -0.091 \\ -0.091 & 0.446 & -1.114 \\ -0.091 & -1.114 & 0.446 \end{pmatrix}$	$\begin{pmatrix} 0.124 & 0.460 & 0.460 \\ 0.460 & 0.124 & 0.460 \\ 0.460 & 0.460 & 0.124 \end{pmatrix}$

[a]From the long wavelength relation:
[b]For Zr-20 Nb, $c_{11} = 1.160\times10^{11}$ Pa, $c_{12} = 0.789\times10^{11}$ Pa, and $c_{44} = 0.316\times10^{11}$ Pa, at 0 K (present paper).
[c]For Zr-20 Nb, $c_{11} = 1.164\times10^{11}$ Pa, $c_{12} = 0.885\times10^{11}$ Pa, and $c_{44} = 0.327\times10^{11}$ Pa, at 300 K (Goasdoue *et al.* Ref. 31).
[d]For pure Zr, $c_{11} = 1.050\times10^{11}$ Pa, $c_{12} = 0.959\times10^{11}$ Pa, and $c_{44} = 0.337\times10^{11}$ Pa, at 915 K (Heiming *et al.* Ref. 27).

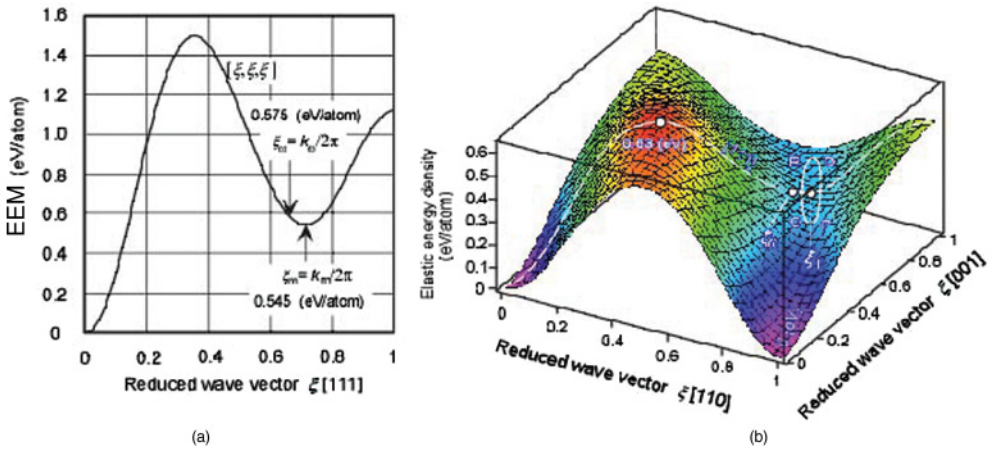

FIG. 3. (Color online) (a) The ω EEM $Y(\mathbf{k}) = a_i a_j \Phi_{ij}(k)/216$ in the $[111]^*$ direction. (b) The elastic strain energy density $\eta_\omega^2 Y(\mathbf{k})$ with $\eta_\omega = 0.653$ in the $(1\bar{1}0)^*$ plane. The ellipse OPQR represents the contour of the half-maximum intensity of the main peak of the defect amplitude square $\tau^2(\mathbf{k} - \mathbf{k}_m)$.

singularity in the general susceptibility function at the Fermi level. The Born-Huang interatomic force constants, $\varphi_{ij}(\mathbf{n})$, can be obtained from the second derivative of the pair potential with respect to the lattice coordinate $\mathbf{n}$. Using the estimated values of $\varphi_{ij}(\mathbf{n})$ in Table I, one can obtain the ω EEM $Y(\mathbf{k})$. Figure 3(a) shows the $Y(\mathbf{k})$ in the Zr-20 Nb alloy plotted against the [111] direction in k space. As anticipated from the phonon dispersion curve of the [111]LA phonon mode, the minimum appears at a point $\mathbf{k}_m$, which deviates from the ideal $\mathbf{k}_\omega$ by $\Delta\mathbf{k}_\omega \sim 0.021\mathbf{k}_\omega$ at higher angles. The deviation in the Zr-20 Nb alloy is held by experimental observations in the range $\Delta\mathbf{k}_\omega = (0.018\text{–}0.023)\mathbf{k}_\omega$ [16,17]

The contour map of the EEM described in k space offers a chance to determine the equilibrium shape of the metastable ω phase.[5,21,25] A distinctive feature of $\eta_\omega^2 Y(\mathbf{k})$ with $\eta_\omega = 0.653$ is obtained in the $(1\bar{1}0)^*$ reciprocal plane, as shown in Fig. 3(b). The minimum point $\mathbf{k}_\omega$ is located at the saddle point in the extended valley. The equal contour of the ellipse OPQR drawn in Fig. 3(b) predicts the half-maximum width of the main peak (cf. Fig. 8) of the defect amplitude square $\tau(\mathbf{k} - \mathbf{k}_m)\tau^*(\mathbf{k} - \mathbf{k}_m)$. It can be converted to the IC ω phase ACTV depicted in Fig. 2. The integration of Eq. (17) in the ellipse OPQR gives the elastic strain energy of the unit cell of the IC ω phase.

The Bain-distortion energy $g^{\mathrm{Bn}}_{\mathrm{elastic}}(\mathbf{k})$ is expressed in terms of the Bain EEM $Z^{\mathrm{Bn}}(\mathbf{k})$ and the shape function $\theta(\mathbf{k})$ as follows:[21–26]

$$g^{\mathrm{Bn}}_{\mathrm{elastic}}(\mathbf{k}) = \tfrac{1}{2} Z^{\mathrm{Bn}}(\mathbf{k})\theta^2(\mathbf{k}), \tag{19}$$

$$Z^{\mathrm{Bn}}(\mathbf{k}) = \Omega\hat{\varepsilon}_{ii} C_{iikk}\hat{\varepsilon}_{kk} - \tfrac{1}{4}\Psi_i^{\mathrm{Bn}}(\mathbf{k})\Phi_{ij}^{-1}(\mathbf{k})\Psi_j^{\mathrm{Bn}}(\mathbf{k}), \tag{20}$$

where C_{ijkl} is the stiffness constant and $g^{\mathrm{Bn}}_{\mathrm{elastic}}(\mathbf{k})_{k\to 0} = g_{\mathrm{strain}}(\varepsilon_{ii})$ in Eq. (A11).

Taking the reverse FT of $g^{\omega}_{\mathrm{elastic}}(\mathbf{k})$ and $g^{\mathrm{Bn}}_{\mathrm{elastic}}(\mathbf{k})$ one can obtain the elastic strain energy in real space as shown in Fig. 4. It is clear from the small volume change $\hat{\varepsilon}_V$ less than 0.01 in the Zr-20 Nb alloy[18,28] that the Bain-distortion energy is negligibly small $[g^{\mathrm{Bn}}_{\mathrm{elastic}} < 10^{-4}(\mathrm{eV/atom})]$ compared to the ω-distortion energy. A similar argument is made about the Bain-gradient term $g^{g}_{\mathrm{strain}}(\varepsilon_{ii})$ of Eq. (1), i.e., Eq. (A13). The Bain-gradient coefficient $\kappa^{\mathrm{Bn}}_{\mathrm{strain}}(\mathbf{k})$ at the Γ point is $\kappa^{\mathrm{Bn}}_{\mathrm{strain}}(\mathbf{k})_{k111\to 0} = 1.24 \times 10^{-3}(\mathrm{eV/nm})$ along the [111] direction and is 0.61×10^{-3} (eV/nm) along the [100] direction, respectively. It is 10^{-4} –10^{-5} orders of magnitude smaller than the ω gradient coefficient.

From the above elastic strain energy calculation, the average strain energy per atom in the IC ω phase is determined to have a constant value $g^{\omega}_{\mathrm{elastic}} = 0.020\,(\mathrm{eV/atom})$ throughout the IC ω embryo over the size $p_{\mathrm{pau}} = 66$. It is a rather natural result because, for the IC ω embryo over the size $p_{\mathrm{pau}} = 66$, we sum up the term $Y(\mathbf{k})\tau^2(\mathbf{k} - \mathbf{k}_m)$ in almost the same region around $\mathbf{k} = \mathbf{k}_m$ [see Figs. 3(a) and 3(b)].

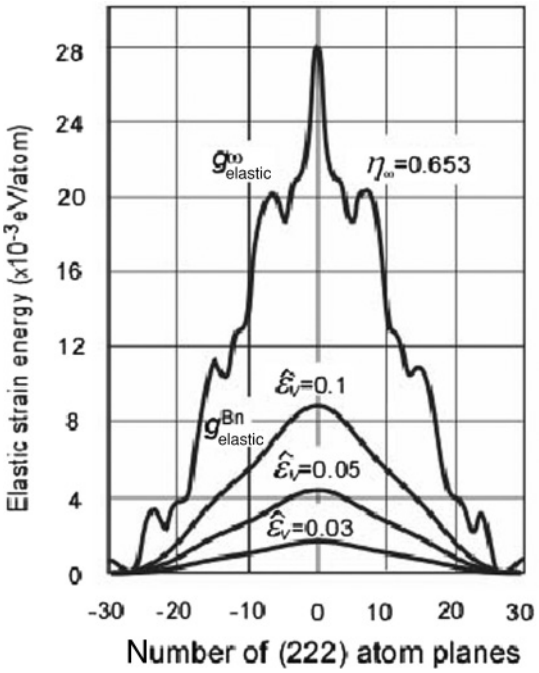

FIG. 4. For the embryo size $p_{\mathrm{pau}} = 102$, the ω-distortion energy $g^{\omega}_{\mathrm{elastic}}(\mathbf{n})$ and the Bain-distortion energy $g^{\mathrm{Bn}}_{\mathrm{elastic}}(\mathbf{n})$ are plotted against the (222) planes. The ω-distortion energy per atom is 0.020 eV/atom.

The interaction energy $g^{\omega-\mathrm{Bn}}_{\mathrm{elastic}}(\mathbf{k})$ of Eq. (16) vanishes because the square of the defect amplitude of the interaction energy is expressed as $\tau(\pm\mathbf{k})\tau(\mathbf{k}\mp\mathbf{k}_\omega)$. Consequently, one may conclude that the elastic strain energy density in the IC ω phase transition is yielded almost entirely from the ω distortion of the IC ω embryo.

C. Gradient strain energy

In addition to the contribution to the interfacial energy associated with the activation barrier of the potential (see Fig. 8), there are gradient energy contributions expressed as $g^{g}_{\mathrm{strain}}(\varepsilon_{ii})$ in Eq. (1) and $g^{g}_{\psi}(\eta)$ in Eq. (3). However, true continuum theory provides no means for estimating the gradient energy contributions, i.e., no means for estimating the coefficients κ, χ, ζ, etc., nominated in the gradient energy terms, Eqs. (A8) and (A13). This can be performed in a straightforward manner with the microscopic theory by expanding the EEM about the origin (Bain distortion) or about $\mathbf{k}_m$ (ω distortion) of reciprocal space to the second order. In the vicinity of the minimum point $\mathbf{k}_m$, the ω EEM exhibits a parabolic form of the curve along the [111] direction as shown in Fig. 3(a). Indeed, expanding to the second order of $\mathbf{k}$ in the [111] direction, we obtain the parabolic curve of the ω EEM as

$$Y(\mathbf{k}) \approx Y(\mathbf{k}_m) + \frac{\kappa^{\omega}_{\mathrm{elastic}}(\mathbf{k}_m)|\hat{\boldsymbol{n}}\cdot(\mathbf{k}-\mathbf{k}_m)|^2}{2}, \tag{21}$$

$$\kappa^{\omega}_{\mathrm{elastic}}(k) = \hat{\boldsymbol{n}}\cdot\nabla_k[\hat{\boldsymbol{n}}\cdot\nabla_k Y(\mathbf{k})], \tag{22}$$

The wave-vector-magnitude dependence of the ω EEM $Y(k)$ obtained from the microscopic elasticity theory yields an elastic gradient energy. It corresponds to the chemical gradient energy of the Cahn-Hilliard theory.[29,30]

On the other hand, the homogeneous gradient energy $\chi(\hat{\boldsymbol{n}}\cdot\nabla\eta)^2/2$ of Eq. (3) is rewritten in a form of the local gradient term using the definition $\eta_\omega(\mathbf{n}) = \eta_\omega\sigma(\mathbf{n})$. Taking the FT of the pseudospin $\sigma(\mathbf{n})$ for atoms, we obtain the local gradient energy in k space as follows:

$$\frac{\chi(\hat{\boldsymbol{n}}\cdot\nabla\eta)^2}{2} = \frac{1}{2}\chi\eta_\omega^2[\hat{\boldsymbol{n}}\cdot(\mathbf{k}-\mathbf{k}_m)]^2\tau^2(\mathbf{k}-\mathbf{k}_m). \tag{23}$$

Comparing the discrete lattice model (microscopic elasticity theory) of Eq. (23) with the homogeneous one of Eq. (21), we find, with the help of Eq. (3), that

$$\begin{aligned}\sum_x\left[-\kappa\hat{\boldsymbol{n}}\cdot\nabla\phi + \left(\frac{\chi}{2}\right)(\hat{\boldsymbol{n}}\cdot\nabla\phi)^2\right]\eta_\omega^2 + \frac{1}{2}\chi \\ \times\sum_k[\hat{\boldsymbol{n}}\cdot(\mathbf{k}-\mathbf{k}_m)]^2\tau^2(\mathbf{k}-\mathbf{k}_m)\eta_\omega^2 \\ = \frac{1}{4}\kappa^{\omega}_{\mathrm{elastic}}(\mathbf{k}_m)\sum_k[(\hat{\boldsymbol{n}}\cdot(\mathbf{k}-\mathbf{k}_m)]^2\tau^2(\mathbf{k}-\mathbf{k}_m)\eta_\omega^2\,(\mathrm{eV/atom}).\end{aligned} \tag{24}$$

Because the term $2\kappa\hat{\boldsymbol{n}}\cdot\nabla\phi$ in Eq. (24) vanishes ($\kappa = 0$) at $\pm\mathbf{k}_m$ and $\phi(\mathbf{n}) = \Delta\mathbf{k}_\omega\cdot\mathbf{n} + \phi^0$ in the PWA, the phenomenological coefficient χ in Eq. (23) is given by

$$4\chi = \kappa^{\omega}_{\mathrm{elastic}}(\mathbf{k}_m). \tag{25}$$

The ω gradient coefficient for the Zr-20 Nb alloy is obtained from Eq. (22) as $\kappa^{\omega}_{\mathrm{elastic}}(\mathbf{k}_m) = 0.0348\,(\mathrm{eV}^{-1}\mathrm{nm}^{-2}\,\mathrm{atom})$, and the phenomenological coefficient χ is estimated as $x = 0.0087\,(\mathrm{eV}^{-1}\,\mathrm{nm}^{-2}\,\mathrm{atom})$. This χ value is adopted for the calculation of Eqs. (7) and (8).

IV. L-L FREE ENERGY OF THE IC ω EMBRYO

In the present IC ω phase transition, finely dispersed IC ω embryos are formed in the parent phase by heterophase fluctuation. The free-energy function of the system, therefore, should have a form reflecting the distribution of the IC ω embryos, each of which is associated with the elastic strain energy.

Following the same procedure as Yamada and co-workers,[4] the free-energy density $g(\eta)$ for the IC ω phase transition is expressed in the L-L expansion form in Appendix B. Taking the dispersed embryos and the associated elastic strain energy into account, we take the FT of Eq. (9) over the crystal,

$$\sigma_{\mathrm{crys}}(\mathbf{k}) = \frac{1}{N}\sum_{n=1}^{N}\sigma(\mathbf{n})\exp[-\mathbf{k}\cdot\mathbf{n}]. \tag{26}$$

Substituting $\phi = 2\pi/3$ in the FT free-energy function, we obtain a Landau type of free energy for the inhomogeneous system as follows:

$$\begin{aligned}G(\eta) = \Bigg\{&\frac{1}{2}\eta^2\sum_k Y(\mathbf{k})\tau^2_{\mathrm{crys}}(\mathbf{k}-\mathbf{k}_m) \\ &+\sum_k\theta^2_{\mathrm{crys}}(\mathbf{k}-\mathbf{k}_\omega)\left[\frac{2}{3}\beta(\mathbf{k}_\omega)\eta^3_{\mathrm{crys}}\right. \\ &\left.+\frac{1}{4}\gamma(\mathbf{k})\eta^4 + \frac{1}{6}\delta(\mathbf{k})\eta^6 - ST\right] \\ &+\frac{1}{2}\sum_k Z^{\mathrm{Bn}}(\mathbf{k})\theta^2_{\mathrm{crys}}(\mathbf{k})\Bigg\}.\end{aligned} \tag{27}$$

where the subscript crys indicates the FT is to be executed over the crystal. The harmonic term coefficient $\alpha(\mathbf{k})$ is replaced by the term $Y(\mathbf{k})\tau^2(\mathbf{k}-\mathbf{k}_m)$ from the relation in Eq. (17). The third-order term $\beta(\mathbf{k}_\omega)$ possesses the unique property that it can be produced only from the $\mathbf{k}_\omega$ wave.[5] The other higher-order terms $\gamma = C(\mathbf{k}_\omega,\mathbf{k}_\omega,\mathbf{k}_\omega,\mathbf{k}_\omega,-\mathbf{k}_\omega)$ and $\delta = D(\mathbf{k}_\omega,\mathbf{k}_\omega,\mathbf{k}_\omega,\mathbf{k}_\omega,\mathbf{k}_\omega,\mathbf{k}_\omega)$ may also be assumed to be independent of the wave vector $\mathbf{k}$ because $\theta(\mathbf{k}-\mathbf{k}_\omega)$ has a finite value only in a small region around $\mathbf{k}_\omega$. From the definition of $\theta_{\mathrm{crys}}(\mathbf{k})$, $\sum_k\theta^2_{\mathrm{crys}}(\mathbf{k}-\mathbf{k}_\omega) = C$, C being the concentration of the IC ω phase, we can express the thermodynamical potential per atom in the IC ω embryo as follows:

$$\begin{aligned}g(\eta) = &\frac{1}{2}\eta^2\sum_k Y(\mathbf{k})\tau^2(\mathbf{k}-\mathbf{k}_m) \\ &+\left[\frac{2}{3}\beta(\mathbf{k}_\omega)\eta^3 + \frac{1}{4}\gamma\eta^4 + \frac{1}{6}\delta\eta^6 - ST\right]\sum_k\theta^2(\mathbf{k}-\mathbf{k}_\omega) \\ &+\frac{1}{2}\sum_k Z^{\mathrm{Bn}}(\mathbf{k})\theta^2(\mathbf{k}).\end{aligned} \tag{28}$$

One should keep in mind that each coefficient $\{a(\mathbf{k}),\beta(\mathbf{k}_m),\gamma,\delta\}$ contains the elastic strain energy yielded by the embryo itself. For example, in the present Zr-20 Nb

alloy, each atom in the IC ω embryo dresses in the elastic strain energy by 0.020 eV/atom. The entropy term $-ST$ is singled out in Eq. (28) to clarify the role of each coefficient $\{a(\mathbf{k}),\beta(\mathbf{k}_m),\gamma,\delta\}$ in the IC ω phase transition. The analytical expression of S in the mean-field approximation is given in Appendix B.

The harmonic term coefficient $a(\mathbf{k})$ and the third-order anharmonic coefficient $\beta(\mathbf{k}_\omega)$ have already been evaluated from the phonon dispersion curve (Fig. 3) and the PWA approximation of phase field $\phi(\mathbf{n})$, respectively. Therefore, to analyze the temperature dependence of the microstructure of the IC ω phase, we must have the numerical values of the other two coefficients $\{\gamma,\delta\}$ of the function (28). Theoretically, a first-principles electronic structure calculation would be necessary, along with an elastic energy calculation, to estimate the free-energy density. However, even if reasonable expressions can be found for the anharmonic coefficients, the task of finding the proper free-energy minimum remains highly nontrivial, as the optimal value of the amplitudes must be found by solving sets of coupled nonlinear integral equations in the displacement of atoms. Therefore, it was inevitable that we obtained the numerical values of the anharmonic coefficients by fitting the curve to experimental values.[2,5] Two unknown parameters γ and δ are obtained by assuming a ground-state total energy difference Δw between the β and the ω phases as $\Delta w = -0.144$ (eV/atom) and the [111]LA phonon frequency v_w as $v_w = 2.0v_\beta$ so as to match the experimental results of the degree of order $\eta_m = 0.64$ at 280 K[16–18] and the transition temperature $T_0 = 280$ K.[5,31] It should be noted that both Δw and n_w could be obtained from the first-principles calculation. That is, all coefficients except $B_0(\mathbf{k}_\omega)$ could be evaluated from the first-principles electronic structure calculation of the ω phase. The obtained values $\gamma = -4.375$ and $\delta = 8.771$ (eV/atom) dress in the elastic strain energy. Therefore, the ground-state potential of the IC ω phase should have a value $\Delta w + g^{\omega}_{\text{elastic}} = -0.124$(eV/atom). The proper construction of the free-energy curve has been judged from the shape of the parabolic curve, viz. from the numerical values of $[\partial^2 f(\eta)/\partial^2\eta]$ at the origin $(\eta = \eta_m)$,[16,18] the activation energy $f(\eta^*)$,[6,24] the temperature dependence of h_w,[18,25] and the shift of the diffuse intensity peak.[16–18]

The L-L free energy $F = p_{\text{pau}} f(\eta)$ is plotted against the degree of order η in Fig. 5 using the evaluated coefficients $\mathbf{a}(\mathrm{k}) = Y(\mathbf{k})\tau^2(\mathbf{k}-\mathbf{k}_m)$, $\beta(\mathbf{k}_\omega) = -0.210$, $\gamma = -4.375$, and $\delta = 8.771$. Stable IC ω embryos are identified from the plotted L-L free energy. They are $p_{\text{pau}} = 102\,[n(222) = 51]$ between 280 and 300 K, $p_{\text{pau}} = 84\,[n(222) = 42]$ between 300 and 400 K, and $p_{\text{pau}} = 66\,[n(222) = 33]$ above 400 K.

The larger embryo $p_{\text{pau}} = 102$ $[Y(\mathrm{k_m}) = 0.545$ eV/atom] exhibits lower free energy than the smaller embryo $p_{\text{pau}} = 66$ at 300 K $[Y(\mathbf{k})_{\text{pau}=66} = 0.550$ eV/atom] (↑ in Fig. 5). This occurred because a minor change in the harmonic modulus $Y(\mathbf{k})$ can have a significant structural effect on the Landau free energy at large η, and at lower temperature, such as 300 K, the contribution of the entropy term $-ST > 0$ is still small. As a result, at 300 K, the embryo $p_{\text{pau}} = 66$ exhibits a higher free energy than $p_{\text{pau}} = 102$.

Sanchez and de Fontaine[15] have tried to understand the unusual circular diffuse scattering observed in Ti and Hf alloys quenched from high temperatures.[32] A plausible atomic displacement field was obtained using a computer simulation to FT a curved intensity streak, mimicking that observed experimentally in electron-diffraction patterns of Ti and Hf alloys. The IC ω phase structure obtained by Sanchez and de Fontaine is reproduced by exhibiting the atom positions and their displacements in the IC ω phase transition. Figure 6 is a reproduction of the data of Sanchez and de Fontaine[15] with the atoms

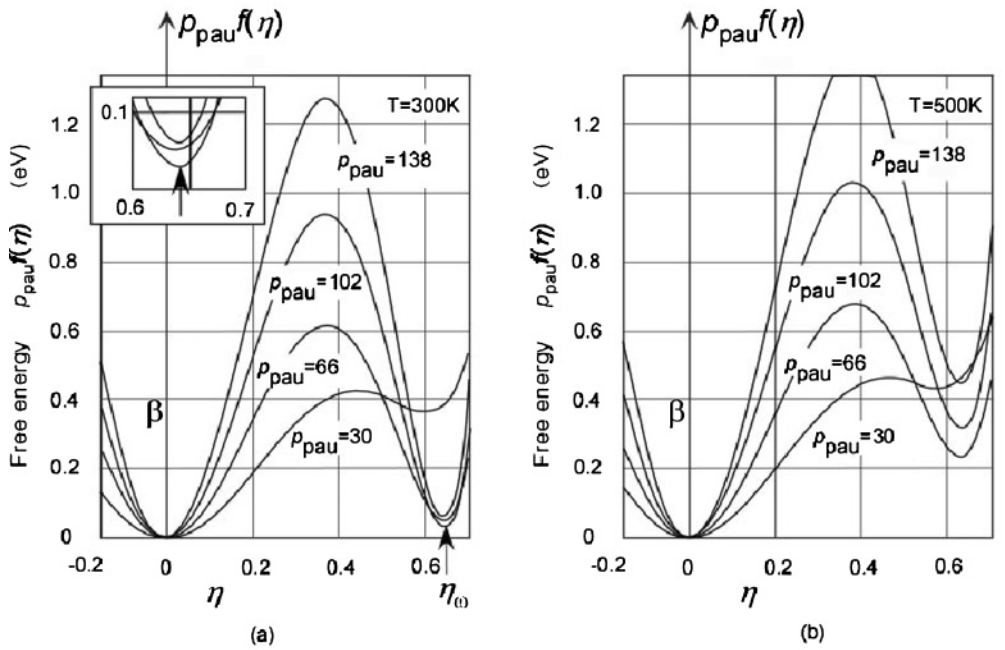

FIG. 5. Landau free energy $p_{\text{pau}} f(\eta)$ is plotted against the degree of order η. (a) At 300 K, the primitive activation unit $p_{\text{pau}} = 102$ has the minimum free energy. (b) At 500 K, $p_{\text{pau}} = 66$ has the minimum free energy.

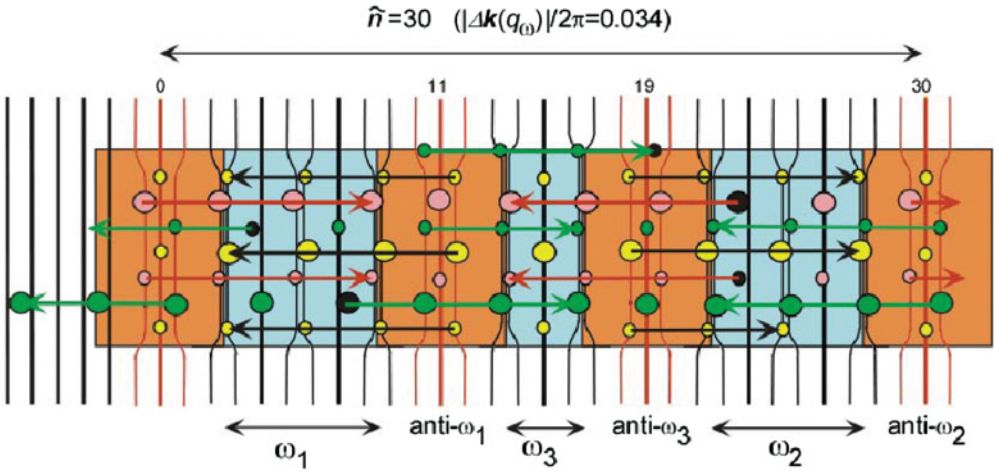

FIG. 6. (Color online) The IC ω phase structure by Sanchez and de Fontaine[15] is reproduced by showing the atom positions as well as their displacements in the IC ω phase transition. Note that the anti-ω phase, instead of β walls, exists as the soliton walls in the embryo.

explicitly exhibiting their positions and displacement fields. The formation of anti-ω walls is in agreement with the microstructural model proposed in the present paper. The smaller size of the unit-cell embryo, i.e., $p_{\rm pau} = 60$, is also in good agreement with our conclusion of high temperatures for the IC ω phase $p_{\rm pau} = 66$. In fact, Sanchez and de Fontaine have explained, "*As the temperature is lowered, the curved streak will tend to straighten out, and the linear defect period increase to approximately 50 A*" (*italic* by Sanchez and de Fontaine[15]). Our microstructural model $p_{\rm pau} = 66$ also seems to be adequate for the IC ω structure at high temperatures close to T_i.

V. DIFFUSE SCATTERING

The microstructure of the IC ω phase may be most directly identified from the spectra of x-ray diffuse scattering. Ignoring the Bain distortion, we obtain the scattering function of the IC ω phase as

$$I_\omega(\mathbf{h}) = I_e p_{\rm pau}^2 \eta^2 z(\mathbf{h}) z(\mathbf{h}) h_i h_j a_i a_j \tau^2(\mathbf{k} \pm \mathbf{k}_m), \quad \mathbf{h} + \mathbf{k} = \mathbf{g}, \tag{29}$$

where $z(\mathbf{h}) = F(\mathbf{h}) \exp[-M(\mathbf{h})] \exp[-R(\mathbf{h})]$ is the dynamical structure factor multiplied by the temperature Debye-Waller factor $M(\mathbf{h})$ and the static displacement factor $R(\mathbf{h})$, respectively.

The calculation is simply made for the essential term $(|\mathbf{h}| p_{\rm pau})^2 \tau^2(\mathbf{k} - \mathbf{k}_m)$ to identify the relevant microstructure of the IC ω phase. The spectra calculated for $p_{\rm pau} = 102$ are given in Figs. 7(a) and 7(b). The IC ω phase is supposed to consist of a sequence of subvariants $\omega 1$-$\omega 3$-$\omega 2$ separated by anti-ω phase walls (bold line) or β phase walls (thin solid line). For comparison, the single-layer soliton model $[n_{\rm wall}(222) = 3]$ and the three-layer soliton model $[n_{\rm wall}^{\rm thick}(222) = 7]$ are

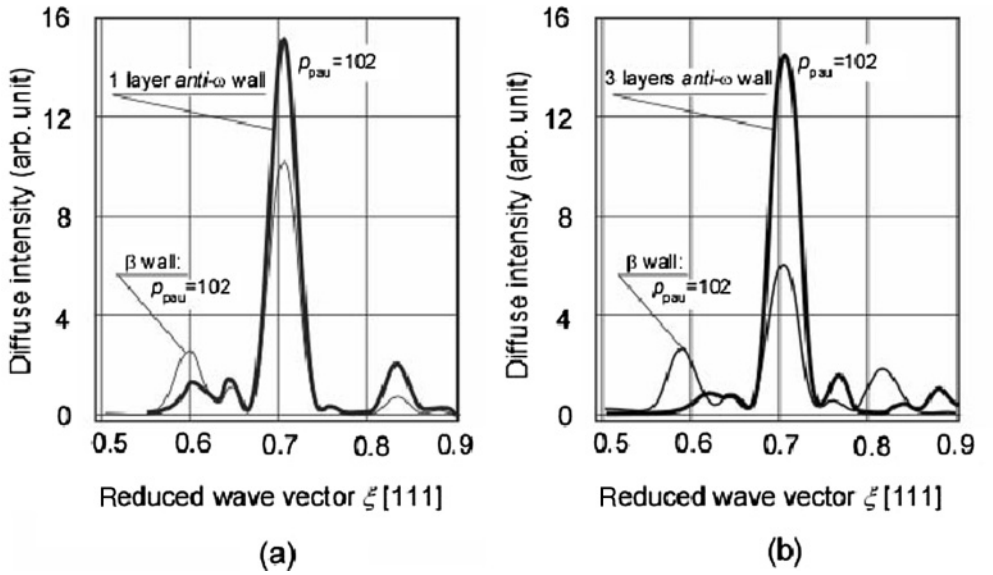

FIG. 7. Diffuse intensity of the IC ω structure is plotted in the [111] direction. (a) Single-layer anti-ω model. (b) Three-layer anti-ω model.

shown in Figs. 7(a) and 7(b), respectively. The anti-ω wall model exhibits a strong main peak at the position $(\mathbf{k}_m) = (0.71,0.71,0.71)$ compared to the β wall model. Satellite peaks also appear, for example, at $(\mathbf{k}_s) = (0.85,0.85,0.85)$ for the single-layer anti-ω wall model and at $(\mathbf{k}_s) = (0.6,0.6,0.6)$ for the β soliton model. In both cases, shown in Figs. 7(a) and 7(b), the soliton wall model consisting of an anti-ω phase structure can account for the experimental results of diffuse intensity.

VI. CONCLUSIONS AND DISCUSSION

The subject we are concerned with is obtaining a pertinent thermodynamical model of the weak first-order phase transition to describe the possible modulated ω phase and to clarify the kinematic stabilizing mechanism that occurs in the metastable ω phase transition.

There are two important factors to be considered in due course in analyzing the metastable ω phase transition. The first is the morphology of the metastable ω phase. Finely dispersed metastable ω particles, which are called IC ω embryos in the text, are formed in the parent phase. The embryos always dress in the elastic strain energy yielded by the constraint of the parent lattice. Therefore, the free-energy functional of the system should be improved to a form that can describe the metastable ω embryos, which always dress in the elastic strain energy in the parent lattice. A group-theory consideration is made to set up the L-L free energy with proper order parameters (σ_i, η, ϕ, etc.). These components are optimized successively to unambiguously identify the size, shape, and microstructure of the metastable ω phase. By applying microscopic elasticity theory to the elastic strain components, the harmonic term of the L-L free energy is expressed as $A(\mathbf{k}_m)\eta^2 \equiv \sum_k Y(\mathbf{k})\tau^2(\mathbf{k}-\mathbf{k}_m)\eta^2$. It is elucidated that the anharmonic coefficients of the L-L free energy, which is expanded up to sixth-order terms, could be evaluated, except for the third-order term, from the first-principles electronic structure calculation.

The second factor is the meaning of the weak first-order phase transition, which is representatively expressed by the third-order term of the L-L expansion of the free energy. By optimizing the thermodynamical potential energy with respect to the phase change $\phi(\mathbf{n})$, the IC ω phase is shown to have a microstructure with subvariant sequence $-\omega1$-$\omega3$-$\omega2-$ separated by the soliton walls of the anti-ω structure. It should be noted that the third-order term has a negative value in the L-L expansion of free energy. This causes characteristic differences in the behavior and the microstructure of the present IC ω structure from the IC structures obtained by even-order transition. This drives the weak first-order transition of the IC ω phase and functions in maintaining a constant width for the soliton walls over the temperature range $T_I > T > T_C$.

The kinematic stabilizing mechanism can be understood most easily by the graphical construction of the L-L free-energy density for the fluctuation structure. The curves for two single-wave structures with $\mathbf{k} = \mathbf{k}_m$ and $\mathbf{k} = \mathbf{k}_\omega$ are sketched in Fig. 8. The free-energy curve with the minimum phonon energy $\mathbf{k}_m$ always lies below the curve with the phonon energy $\mathbf{k}_\omega$ for the pure ω phase, viz., the harmonic term $\alpha(\mathbf{k}_m)\eta^2 < \alpha(\mathbf{k}_\omega)\eta^2$ in the L-L expansion. For this lower free-energy curve, the sinusoidal standing wave,

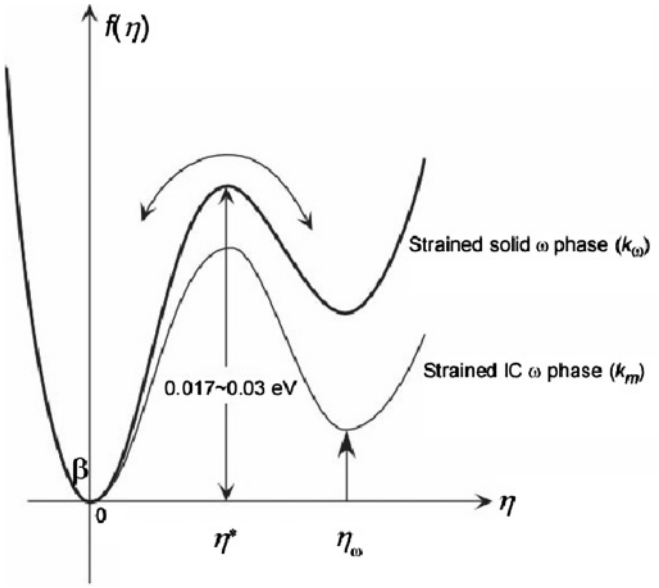

FIG. 8. Potential curves for the two transformation waves with the wave vectors $\mathbf{k}_m$ and $\mathbf{k}_\omega$ are depicted as a function of the displacement ordering parameter η. The activation energy is adopted from Refs. 6 and 29.

$\psi_{\mathrm{IC}\omega}^{\mathrm{PWA}} = \eta_\omega \exp[-i\phi(\Delta\mathbf{k}_m \cdot \mathbf{n})] \sin(\mathbf{k}_\omega \cdot \mathbf{n})$ with the wave vector $\mathbf{k}_m$, develops; however, at the same time, a competition occurs between this initial harmonic wave $\mathbf{k}_m$ and the nonvanishing third-order term with the wave vector $\mathbf{k}_\omega$. This results in the decomposition of the $\mathbf{k}_m$ wave into the modulated ω structure with the subvariants $-\omega1$-$\omega3$-$\omega2-$ separated by the soliton walls of the anti-ω structure.

We have obtained the stable modulated ω phase, which could be depicted in a phase diagram from the analysis of the L-L free energy and the numerical calculations. They are $p_{\mathrm{pau}} = 102[(n(222) = 51]$ between 280 and 300 K, $p_{\mathrm{pau}} = 84[(n(222) = 42]$ between 300 and 400 K, and $p_{\mathrm{pau}} = 66[(n(222) = 33]$ above 400 K. X-ray and neutron-diffraction experiments[11,16,17] have demonstrated the existence of modulated ω embryos far above the solid ω phase starting temperature T_0. It is instructive to refer to the electron-diffraction patterns[33] taken from the quenched β (bcc) phase of the Ag-24.1 at . % Al alloy in Fig. 9 (so far, there has been no report on the circular diffuse intensity in Zr-Nb alloys). The circular diffuse intensities of the Ag-Al alloy are separately exhibited from those of the scattered ellipsoidal peaks of the modulated ω embryos. It is important to note that the circular diffuse intensity observed in the β parent phase remains in the martensite phase formed upon cooling.[33] As understood from Fig. 4, the meaningful value of the Bain-interaction energy could only be obtained by the stress-free strain, which is as large as $\hat{\varepsilon}_{ii}^{\mathrm{Bn}-1}\hat{\varepsilon}_{kk}^{\mathrm{Bn}-2} > 0.01$ This condition would be attained from the combination of a vacancy (Bn$-$1) and a ω lattice (Bn$-$2) but would not be attained by the interaction of the metastable ω phase variants. Therefore, it is clear that certain types of defects, such as vacancies or impurities, trap the metastable ω embryo formed at higher temperatures.

Two different sizes of the modulated ω phase, which are pinned at higher temperatures and are unpinned at lower temperatures, are simultaneously quenched in at room

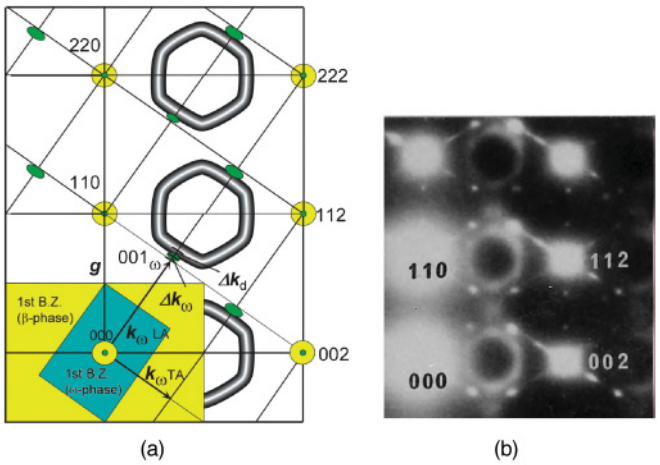

FIG. 9. (Color online) (a) Schematic of diffuse scattering intensities of a single 111 variant of the IC ω phase in the $(1\bar{1}0)^*$ plane. (b) Diffraction pattern of $(1\bar{1}0)^*$ zone taken from the quenched β phase of the Ag-24.1 at.% Al alloy.

temperature (RT) in the Ag-Al alloy. Therefore, we can say that the circular diffuse intensity analyzed by Sanchez and de Fontaine[15] represents the quenched metastable ω embryos pinned by the point defects at high temperatures. That is, at high temperatures above 400 K, the metastable ω embryos $p_{\text{pau}} = 66[(n(222) = 33]$ may be formed in the Zr-20 Nb alloy. On the other hand, the scattered ellipsoidal peaks in Fig. 9 suggest the existence of unpinned IC ω embryos $p_{\text{pau}} = 102[(n(222) = 51]$ at RT in the Zr-20 Nb alloy.

APPENDIX A: ORDER PARAMETERS OF THERMODYNAMICAL POTENTIAL-ENERGY DENSITY IN THE IC ω PHASE TRANSITION

We determine the transformation properties under the action of the bcc space-group symmetry so that the correct form of the thermodynamical potential-energy density may be constructed. The space group of the present bcc alloy is $Im\bar{3}m$, and the generators of this group may be taken to be (i) the bcc primitive translation vectors and (ii) the elements I, C_3, and C_4. The transformation occurs by the transformation wave of the LA mode with the wave vector $\mathbf{k}_\Lambda = \xi(1,1,1)$. The k_Λ space group, corresponding to the Λ line of the first Brillouin zone, is given by $G_0(\mathbf{k}_\Lambda) = \{E, 2C_3, 2C_2', I, 2S_6, 3\sigma_d\}$.

The product ω phase has the symmetry of space group $R\bar{3}m$, and the irreducible representation A_{1g} of this space group has a compatibility relation to T_{2g} and A_{1g} of the space group $Im\bar{3}m$, where the A_{1g} ($\mathbf{k}_\Lambda^1$) phonon is responsible for the normal coordinate of the [111]LA phonon mode of the bcc alloy. The star of $\mathbf{k}_\Lambda$ may be denoted by $\pm\mathbf{k}_\Lambda^\lambda$ ($\lambda = 1,\ldots,4$), where $\mathbf{k}_\Lambda^1 = \xi(1,1,1)$, $\mathbf{k}_\Lambda^2 = \xi(\bar{1},1,1)$, $\mathbf{k}_\Lambda^3 = \xi(1,\bar{1},1)$, and $\mathbf{k}_\Lambda^4 = \xi(1,1,\bar{1})$. Here, we introduce proper order parameters (normal coordinates) $Q_1,\ldots, Q_4$ with $Q_\lambda = \eta\lambda e^{-i\phi_\lambda}$, according to

$$\mathbf{u}_\lambda(\mathbf{n}) = \eta_\lambda \hat{\mathbf{k}}_\Lambda^\lambda \sin\left(\mathbf{k}_\Lambda^\lambda \cdot \mathbf{n} + \phi_\lambda\right) = (i/2)\hat{\mathbf{k}}_\Lambda^\lambda Q_\lambda \times \exp\left(-\mathbf{k}_\Lambda^\lambda \cdot \mathbf{n}\right) + \text{c.c.} \quad (\lambda = 1-4), \tag{A1}$$

where $\hat{\boldsymbol{k}}_\Lambda^\lambda$ is the unit vector in the λ direction in reciprocal space. The phase angle $\phi\lambda$ describes the phase due to the deviation of the minimum point $\mathbf{k}_m^\lambda$ from the ideal ω point $\mathbf{k}_\omega^\lambda$, and, in the PWA, it is defined as follows:

$$\phi_\lambda = \Delta\mathbf{k}_\omega^\lambda \cdot \mathbf{n} + \phi_0, \tag{A2}$$

under PWA. Thus, we find

$$\{E|n\}Q_\lambda \to Q_\lambda \exp\left(-i\left\{\mathbf{k}_\Lambda^j \cdot \mathbf{n}\right\}\right), \tag{A3}$$

$$\{I|0\}Q_\lambda \to Q_\lambda^*, \tag{A4}$$

$$\{C_{3[111]}^+|0\}\begin{pmatrix} Q_1 \\ Q_2 \\ Q_3 \\ Q_4 \end{pmatrix} = \begin{pmatrix} Q_1 \\ Q_3 \\ Q_4 \\ Q_2 \end{pmatrix},$$

$$(C_{3[111]}^+)^{-1}(x,y,z) \to (z,x,y), \tag{A5}$$

$$\{C_{4z}^+|0\}\begin{pmatrix} Q_1 \\ Q_2 \\ Q_3 \\ Q_4 \end{pmatrix} = \begin{pmatrix} Q_2 \\ Q_4^* \\ Q_1 \\ Q_3^* \end{pmatrix},$$

$$(C_{4z}^+)^{-1}(x,y,z) \to (-y,x,z), \tag{A6}$$

Atomic displacements $\mathbf{u}_\lambda(\mathbf{n})$ within the unit cell, which describe intracellular distortions with short wavelengths, are separated into a rapid spatial variation part $\exp[-i\mathbf{k}_\Lambda^\lambda \cdot \mathbf{n}]$ and a relatively slow varying part $Q_\lambda = \eta_\lambda \exp[-i\phi\lambda(\mathbf{n})]$.

The structural transformation involves the intercellular distortions ε_{ij} ($i,j = x,y,z$), which are rewritten in terms of the linear combinations as $\varepsilon_V = \varepsilon_{xx} + \varepsilon_{yy} = \varepsilon_{zz}$ (basis of A_{1g}), $\varepsilon_{1\bar{1}0} = \sqrt{3}(\varepsilon_{xx} - \varepsilon_{yy})$ (basis of E_g), $\varepsilon_{\bar{1}\bar{1}2} = 2\varepsilon_{zz} - \varepsilon_{xx} - \varepsilon_{yy}$ (basis of E_g), and $\varepsilon_4 = \varepsilon_{xy}, \varepsilon_{yz}, \varepsilon_{zx}$ (basis of T_{2g}). The displacement $\varepsilon_{\bar{1}\bar{1}2}$ represents shear strains of the $\{\bar{1}\bar{1}2\}$ planes in the $\pm\langle 111\rangle$ direction. The thermodynamical potential-energy density $g(\eta_j, \phi_j, \varepsilon_{ij})$ is expressed in terms of g_Q, g_Q^g, g_{strain}, g_{strain}^g and $g_{Q-\text{strain}}$ in summation form

$$g(\eta_\lambda,\phi_\lambda,\varepsilon_{ij}) = g_Q(\eta_\lambda,\phi_\lambda) + g_Q^g(\eta_\lambda) + g_{\text{strain}}(\varepsilon_{ij}) + g_{\text{strain}}^g(\varepsilon_{ij}) + g_{Q-\text{strain}}(\eta_\lambda,\varepsilon_{ij}), \tag{A7}$$

where g_Q is the thermodynamical potential-energy density expressed in terms of the proper component Q_λ and Q_λ^*.

Appling the invariant analysis to all terms up to the sixth order in Q_λ, we find

$$\begin{aligned}
&\sum_n^4 g_Q(\eta_n,\phi_n) \\
&= \sum_{\lambda=1}^4 \left\{ \frac{1}{2}A_0 Q_\lambda Q_\lambda^* + \frac{1}{3}B_0\left[Q_\lambda^3 + (Q_\lambda^*)^3\right] \right. \\
&\quad + \frac{1}{4}C(Q_j Q_j^*)^2 + \frac{1}{5}E_0 Q_j Q_j^*\left[Q_j^3 + (Q_j^*)^3\right] \\
&\quad \left. + \frac{1}{6}D(Q_j Q_j^*)^6 + \frac{1}{6}D\left[Q_j^6 + (Q_j^*)^6\right] \right\} \\
&\quad + \sum_{\lambda=1}^4 \sum_{\kappa=1}^{4\,\prime} \left[\frac{1}{4}C_1 Q_\lambda Q_\lambda^* Q_k Q_\kappa^* + \frac{1}{6}D_2 (Q_\lambda Q_\lambda^*)(Q_k Q_\kappa^*)^2 \right] \\
&\quad + \sum_{l=1}^4 \sum_{\lambda}^4 \sum_{k}^{4\,\prime\prime} \frac{1}{6}D_3 (Q_\lambda Q_\lambda^*)(Q_k Q_\kappa^*)(Q_l Q_l^*).
\end{aligned} \tag{A8}$$

The characteristics of the function (A8) are the existence of the third-order anharmonic term $B_0\{Q_j^3+(Q_j^*)^3\}$ that elucidates the first-order phase transition, and no phase-(ϕ)-dependent terms appear in the second-order ($n=2$) and fourth-order ($n=4$) terms of Q_i. This is derived from the antisymmetric transformation wave described by the sine wave of Eq. (A1). The gradient term for the ω phase transformation is

$$\begin{aligned} g_Q^g(\eta_{\sum_\lambda}) = -\frac{\kappa}{2} i \sum_{\lambda=1}^{4} (Q_\lambda^* \hat{\boldsymbol{n}}_\lambda \cdot \nabla_\lambda Q_\lambda - Q_\lambda \hat{\boldsymbol{n}}_\lambda \cdot \nabla_\lambda Q_\lambda^*) \\ + \frac{\chi}{2} \hat{\boldsymbol{n}}_\lambda \cdot \nabla_\lambda Q_\lambda^* \hat{\boldsymbol{n}}_\lambda \cdot \nabla_\lambda Q_\lambda \\ + \frac{\varsigma}{2} Q_\lambda Q_\lambda^* \hat{\boldsymbol{n}}_\lambda \cdot \nabla_\lambda Q_\lambda \hat{\boldsymbol{n}}_\lambda \cdot \nabla_\lambda Q_\lambda^*) \\ (\kappa > 0, \chi > 0, \zeta > 0), \end{aligned} \tag{A9}$$

where $\hat{\boldsymbol{n}}_\lambda$ is the unit vector in the $\lambda = 1$–4 direction. The antisymmetric part of the gradient term, i.e., $Q_\lambda^* \hat{\boldsymbol{n}}_\lambda \cdot \nabla_\lambda Q_\lambda - Q_\lambda \hat{\boldsymbol{n}}_\lambda \cdot \nabla_\lambda Q_\lambda^*$, is the Lifshitz term in the thermodynamical potential-energy expansion.

Applying similar analysis to the distortion, we find the strain energy density g_{strain} up to the sixth order,

$$g_{\text{strain}}(\varepsilon_{ij}) = g_{\text{strain}}^{A1g+Eg}(\varepsilon_{ij}) + g_{\text{strain}}^{T2g}(\varepsilon_{ij}), \tag{A10}$$

$$\begin{aligned} g_{\text{strain}}^{A1g+Eg}(\varepsilon_{ij}) = \frac{c_{11}}{2}(\varepsilon_{xx}+\varepsilon_{yy}+\varepsilon_{zz})^2 \\ -(c_{11}-c_{12})(\varepsilon_{xx}\varepsilon_{yy}+\varepsilon_{yy}\varepsilon_{zz}+\varepsilon_{zz}\varepsilon_{xx}) \\ + c'(\varepsilon_{xx}+\varepsilon_{yy}+\varepsilon_{zz})^4 \\ + c''[(2\varepsilon_{xx}-\varepsilon_{yy}-\varepsilon_{zz})^4 + 9(\varepsilon_{xx}-\varepsilon_{yy})^4] \\ + c'''(\varepsilon_{xx}+\varepsilon_{yy}+\varepsilon_{zz})^6 \\ + c''''[(2\varepsilon_{xx}-\varepsilon_{yy}-\varepsilon_{zz})^6 + 27(\varepsilon_{xx}-\varepsilon_{yy})^6]. \end{aligned} \tag{A11}$$

The first term on the RHS represents the elastic energy, which is responsible for the volume change in the transformation. The second term is responsible for the shear of the $\{110\}$ planes,

$$\begin{aligned} g_{\text{strain}}^{A2g}(\varepsilon_{ij}) = \frac{c_{44}}{2}\left(\varepsilon_{xy}^2+\varepsilon_{yz}^2+\varepsilon_{zx}^2\right) \\ + \beta'_{\varepsilon_{xy}\varepsilon_{yz}\varepsilon_{zx}} + \gamma'\left(\varepsilon_{xy}^4+\varepsilon_{yz}^4+\varepsilon_{zx}^4\right) \\ + \gamma''\left(\varepsilon_{xy}^2\varepsilon_{yz}^2+\varepsilon_{yz}^2\varepsilon_{zx}^2+\varepsilon_{zx}^2\varepsilon_{xy}^2\right) + \beta''\varepsilon_{xy}^2\varepsilon_{yz}^2\varepsilon_{zx}^2 \\ + \gamma'''\left(\varepsilon_{xy}^6+\varepsilon_{yz}^6+\varepsilon_{zx}^6\right) \\ + \gamma''''\left(\varepsilon_{xy}^4\varepsilon_{yz}^2+\varepsilon_{yz}^4\varepsilon_{zx}^2+\varepsilon_{zx}^4\varepsilon_{xy}^2\right) \\ + \gamma'''''\left(\varepsilon_{xy}^2\varepsilon_{yz}^4+\varepsilon_{yz}^2\varepsilon_{zx}^4+\varepsilon_{zx}^2\varepsilon_{xy}^4\right). \end{aligned} \tag{A12}$$

One may remark that g_{strain}^{T2g} can have a characteristic form, even up to the fourth-order term, as $g_{\text{strain}}^{T2g} = g_0 + \alpha r^2 + \beta r^3 + \gamma r^4 + \delta r^6$ for $r = \varepsilon_{xy} = \varepsilon_{yz} = \varepsilon_{zx}$, and it exhibits a double minimum curve with respect to the coordinate r. The gradient term of the strain energy is

$$\begin{aligned} g_{\text{strain}}^{g}(\varepsilon_{ij}) \\ = -\frac{\kappa'}{2}\left(\varepsilon_{yz}\frac{\partial\varepsilon_{zx}}{\partial z} - \varepsilon_{zx}\frac{\partial\varepsilon_{yz}}{\partial z}\right) + \frac{\chi'}{2}\left[\left(\frac{\partial\varepsilon_{yz}}{\partial z}\right)^2 + \left(\frac{\partial\varepsilon_{zx}}{\partial z}\right)^2\right] \\ + \frac{\chi''}{2}\frac{\partial\varepsilon_{yz}}{\partial z}\frac{\partial\varepsilon_{zx}}{\partial z} + \frac{\chi'''}{2}\left[\left(\frac{\partial\varepsilon_{xx}}{\partial x}\right)^2 + \left(\frac{\partial\varepsilon_{yy}}{\partial y}\right)^2 + \left(\frac{\partial\varepsilon_{zz}}{\partial z}\right)^2\right] \\ (\kappa' > 0, \chi', \chi'', \chi''' > 0). \end{aligned} \tag{A13}$$

Including the lowest-order coupling term between ε_{ij} ($i,j = x,y,z$) and the second-order term $(1/2)\sum_{j=1}^{4} A Q_\lambda Q_\lambda^*$, we find the interaction term $g_{Q-\text{strain}}(\eta_{\sum_\lambda}, \varepsilon_{iz})$ as follows:

$$\begin{aligned} g_{Q-\text{strain}}(\eta_{\sum\lambda}, \varepsilon_{ij}) \\ = \sum_{\lambda=1}^{4}\Big[\big\{A_{\text{Bn}-Q}(\varepsilon_{xx}+\varepsilon_{yy}+\varepsilon_{yy})Q_\lambda Q_\lambda^* \\ + A'_{\text{Bn}-Q}\left(\varepsilon_{xx}^2+\varepsilon_{yy}^2+\varepsilon_{zz}^2\right)Q_\lambda Q_\lambda^* \\ + A''_{\text{Bn}-Q}(\varepsilon_{xx}\varepsilon_{yy}+\varepsilon_{yy}\varepsilon_{zz}+\varepsilon_{zz}\varepsilon_{xx})Q_\lambda Q_\lambda \\ + B_{4-Q}\left(\varepsilon_{xy}^2+\varepsilon_{yz}^2+\varepsilon_{zx}^2\right)\big\}Q_\lambda Q_\lambda^* \\ + B'_{4-Q}(\varepsilon_{xx}+\varepsilon_{yy}+\varepsilon_{yy})\left\{Q_\lambda^3+(Q_\lambda^*)^3\right\}\Big]. \end{aligned} \tag{A14}$$

It should be noted that the strain interaction between ε_{ij} and η_λ can occur in the terms above the third order, i.e., $A_{\text{Bn}-Q} \neq 0$.

APPENDIX B: MICROSCOPIC DESCRIPTION OF L-L FREE ENERGY IN THE ω PHASE TRANSITION

We consider a multibody interaction and a grand canonical ensemble. Following the same procedure as Yamada and co-workers,[4] we obtain a microscopic description of the L-L free energy in the ω phase transformation. As the starting point, we give the pseudospin Hamiltonian $H\{\sigma_i\}$, which is obtained by retaining only the kinematical variable σ_i in $H\{\theta_j, \sigma_i\}$. The pseudospin Hamiltonian $H\{\sigma_i\}$ for a system is given by

$$\begin{aligned} H\{\sigma_i\} = {\sum_{ij}}' \varphi_{ij}\sigma_i\sigma_j + {\sum_{ijk}}' \varphi_{ijk}\sigma_i\sigma_j\sigma_k + \cdots - \mu\sum_i \sigma_i, \\ (\sigma_i = -1,0,1), \end{aligned} \tag{B1}$$

where μ is the chemical potential of the atoms. The primes to the summation symbols indicate that no identical numerical numbers are allowed in the summations. The pseudospin σ_i and energy coefficients φ_{ij},φ_{ijk} are the abbreviated form of $\sigma(n_i)$ and coefficients $\varphi(n_i,n_j)$,$\varphi(n_i,n_j,n_k)$, respectively.

In the mean-field theory for the pseudospin $\sigma_i = -1, 0, 1$, the grand partition function of the system $\Xi\{<\sigma>\}$ is given by

$$\begin{aligned} \Xi\{\langle\sigma\rangle\} = \exp(\beta J_1)\{1+2\cosh[\beta(J_2+\mu)]\}^N, \\ \beta = (k_B T)^{-1}, \end{aligned} \tag{B2}$$

$$J_1 = +{\sum_{ij}}' \varphi_{ij}\eta^2 + 2{\sum_{ijk}}' \varphi_{ijk}\eta^3 + \cdots, \tag{B3}$$

$$J_2 = -2{\sum_{ij}}' \varphi_{ij}\eta - 3{\sum_{ijk}}' \varphi_{ijk}\eta^2 - \cdots, \tag{B4}$$

where η is defined as $\eta \equiv \langle\sigma\rangle$ using the ensemble average of the kinematical variable σ_i. N is the number of lattice sites in the crystal. The ensemble average of the kinematical variable σ_i is obtained through $\eta = \partial \ln(\Xi)/\partial(N\beta\mu)$ as

$$\eta = \frac{2\beta \sinh[\beta(J_2+\mu)]}{1+2\cosh[\beta(J_2+\mu)]}, \tag{B5}$$

This self-consistent equation is solved with respect to the chemical potential μ as

$$\mu = -J_2 + \beta^{-1} \ln\left[-\frac{\eta \pm\sqrt{-3\eta^2+4}}{2(\eta-1)}\right]. \tag{B6}$$

Eliminating μ from Eq. (B2), we obtain the mean-field free-energy density as follows:

$$f(\eta) = \frac{1}{N}J_1 + \frac{1}{N}k_BT\int_0^{\eta} \ln\left[-\frac{\eta+\sqrt{-3\eta^2+4}}{2(\eta-1)}\right]d\eta. \tag{B7}$$

The potential function J_1 involves higher-order terms of the interaction potentials. The entropy term is represented by the second term in the integral form. It is expanded in a power series as

$$S = -k_B\sum_{n=1}^{\infty}\left(\frac{3}{4}\right)^{2n-1}\eta^{2n}, \tag{B8}$$

with even powers of η.

[1] K.-M. Ho, C.-L. Fu, and B. N. Harmon, Phys. Rev. B **29**, 1575 (1984).
[2] D. de Fontaine, Met. Trans. A **19**, 169 (1988).
[3] J. A. Krumhansl and R. J. Gooding, Phys. Rev. B **39**, 3047 (1989).
[4] Y. Yamada, Materials Trans. **33**, 191 (1992); K. Fuchizaki, Y. Noda, and Y. Yamada, Phys. Rev. B **39**, 9260 (1989); Y. Yamada and K. Fuchizaki, *ibid.* **42**, 9420 (1990); Y. Yamada, Y. Noda, and K. Fuchizaki, *ibid.* **42**, 10405 (1990).
[5] H. E. Cook, Acta Metall. **22**, 239 (1974); **23**, 1027, 1041 (1975).
[6] H. E. Cook and W. J. Pardee, Acta Metall. **11**, 1403 (1977).
[7] P. Bak and J. von Boehm, Phys. Rev. B **21**, 5297 (1980); Rep. Prog. Phys. **45**, 587 (1982).
[8] D. de Fontaine and J. Kulik, Acta Metall. **33**, 145 (1984).
[9] R. Pynn, J. Phys. F **8**, 1 (1978).
[10] B. Horovitz, J. L. Murray, and J. A. Krumhansl, Phys. Rev. B **18**, 3549 (1978).
[11] B. Borie, S. L. Sass, and A. Anderson, Acta Crystallogr. A **29**, 585 (1973).
[12] For example, R. Blinc, P. Prelovsek, V. Rutar, J. Seliger, and S. Zumer, in *Incommensurate Phases in Dielectrics 1*, edited by R. Blinc and A. P. Levanyuk (North-Holland, Amsterdam, 1986) p. 143; H. Z. Cummins, Phys. Rep. **185**, 211 (1990).
[13] For example, R. J. Gooding and J. A. Krumhansl, Phys. Rev. B **38**, 1695 (1988).
[14] R. Blinc, V. Rutar, B. Topic, F. Milia, and T. Rasing, Phys. Rev. B **33**, 1721 (1986).
[15] J. M. Sanchez and D. de Fontaine, J. Appl. Crystallogr. **10**, 220 (1977).
[16] D. T. Keating and S. J. LaPlaca, J. Phys. Chem. Solids **35**, 879 (1974).
[17] S. C. Moss, D. T. Keating, and J. D. Axe, *Neutron Study of the Beta-to-Omega Instability, Conference on Phase Transitions* (Oxford, Pergamon, London, 1973).
[18] C. W. Dawson and S. L. Sass, Metall. Trans. **1**, 2225 (1970).
[19] G. Papavassiliou, A. Anagnostopoulos, F. Milia, R. Blink, and S. Kotsios, Phys. Rev. B **44**, 7283 (1991).
[20] H. Z. Cummins, Phys. Rep. **185**, 211 (1990).
[21] A. G. Khachaturyan, *Theory of Structural Transition in Solids* (Wiley, New York, 1983), p. 293.
[22] H. E. Cook and D. de Fontaine, Acta Metall. **17**, 915 (1969).
[23] H. Kubo, Phys. Rev. B **32**, 4697 (1985).
[24] D. de Fontaine and O. Buck, Philos. Mag. **27**, 967 (1973).
[25] S. Farjami and H. Kubo, Acta Mater. **56**, 299 (2008).
[26] H. Kubo, Acta Mater. **44**, 4631 (1996).
[27] A. Heiming, W. Petry, J. Trampenau, M. Alba, C. Herzig, H. R. Schober, and G. Vogl, Phys. Rev. B **43**, 10948 (1991).
[28] S. K. Sikka, Y. K. Vohra, and R. Chidambaram, *Omega Phase in Metals: Progress in Materials Science* (Pergamon, New York, 1982), Vol. 27, p. 245.
[29] J. W. Cahn and J. E. Hilliard, J. Chem. Phys. **28**, 258 (1958).
[30] H. E. Cook, Phys. Rev. B **15**, 1477 (1977).
[31] C. Goasdoue, P. S. Ho, and S. L. Sass, Acta Metall. **20**, 725 (1971).
[32] D. de Fontaine, N. E. Paton, and J. C. Williams, Acta Metall. **19**, 1153 (1971).
[33] H. Kubo, S. Hamabe, and K. Shimizu, Scr. Metall. **10**, 548 (1976).